Int. J. Solids Structures Vol. 15, pp. 221–240

0020-7683/79/0301-0221/$02.00/0

DYNAMIC PLASTIC ANALYSIS USING STRESS RESULTANT FINITE ELEMENT FORMULATION

PANITAN LUKKUNAPRASIT

Chulalongkorn University, Bangkok, Thailand

and

JAMES M. KELLY

University of California, Berkeley, CA 94720, U.S.A.

(*Received* 28 *November* 1977; *in revised form* 5 *July* 1978)

Abstract—A stress resultant finite element formulation is developed for the dynamic plastic analysis of plates and shells of revolution undergoing moderate deformation. A nonlinear elastic-viscoplastic constitutive relation simulates the behavior of rate-sensitive and -insensitive materials. A local time step subdivision procedure is developed to stabilize the direct numerical integration of the system of nonlinear dynamic equations; satisfactory accuracy is obtained with large time steps. The simple nonlinear viscoplastic constitutive model approximates the nonlinear dynamic behavior of metals over a wide range of strain rates and has the advantage that the need to identify the state of the material during deformation is eliminated and the numerical algorithm thereby simplified. Direct step-by-step integration techniques are used to solve the system of equations governing the motion of a structure under dynamic loading. An implicit Runge–Kutta scheme in conjunction with a Newton–Raphson iteration technique is used in solving systems of first order ordinary differential equations.

1. INTRODUCTION

The dynamic plastic analysis of structures and continua is a topic undergoing intense development at the present time, stimulated by the need to design structures and components in nuclear power plants against internal accident or external impact, and ductile structures against major earthquakes. Research in this area has been primarily in developing large finite element programs in which equations of motion and constitutive equations of plasticity are integrated using certain well-established numerical techniques. When substantial plastic deformation is involved, the cost and storage requirements of such programs can be prohibitive in the initial design phase, primarily due to difficulties in locating the regions of yielding and in verifying at each point and at each time whether loading or unloading is occurring. An approach affording considerable reduction in computer time and storage is proposed here. The approach is based on a modeling of plastic response in which the need to locate the yielded region and to verify whether loading or unloading is occurring is eliminated. A further simplification of the method when applied to structures composed of rods, beams, plates, or shells is achieved by formulating the yield conditions in stress resultants rather than in stresses, thereby eliminating the need to integrate stress components through the element thickness. The development of this approach to dynamic plastic analysis was motivated by recent research on the utilization of energy-absorbing devices in aseismic design. Since these devices experience substantial plastic deformation and the type currently under study operates in combined torsion and bending, the stress resultant formulation proposed here is highly useful.

The stress resultant finite element formulation proposed herein is developed for the dynamic plastic analysis of plates and shells of revolution undergoing moderate deformation. A nonlinear elastic viscoplastic constitutive relation simulates the behavior of rate-sensitive and -insensitive materials. A local time step subdivision procedure is developed to stabilize the direct numerical integration of the system of nonlinear dynamic equations; satisfactory accuracy is obtained with large time steps.

The principle of virtual work and a finite element discretization technique are used to establish a general finite element displacement formulation for the analysis of structures undergoing large deformation. Two solution approaches are suggested: (1) a current state

formulation in which nonlinear effects are separated, and (2) an incremental formulation. These methods are then specialized to problems of thin plates and shells of revolution subjected to axisymmetric loading and undergoing moderate deformation by employing the Kirchhoff–Love kinematic assumptions and assuming that the material is elastic-perfectly viscoplastic and obeys the von Mises flow condition. Direct step-by-step integration techniques are used to solve the system of equations governing the motion of a structure under dynamic loading. An implicit Runge–Kutta scheme in conjunction with a Newton–Raphson iteration technique is used in solving systems of first order ordinary differential equations.

2. CONSTITUTIVE RELATIONS FOR ELASTIC-VISCOPLASTIC MATERIALS

Only problems in which moderate deformation with small rotations occur will be considered. Therefore, the influence of rotations on constitutive relations is ignored for simplicity and infinitesimal constitutive theory is employed. The error thus introduced is believed to be negligible for practical purposes.

Numerous constitutive theories of elastic-viscoplastic materials for small deformation have been developed[1–8]. Sokolovsky[1] introduced a linear viscoplastic law in which the total strain rate $\dot{\epsilon}$ is assumed to be composed of an elastic part $\dot{\epsilon}^e$ given by Hooke's Law and a viscoplastic part $\dot{\epsilon}^P$ which is proportional to an overstress. A general relation was proposed by Malvern[2] in which the plastic strain rate is assumed to be some function of the current stress and strain. Dislocation theories have been used to develop constitutive models[3, 4]. One such model, suggested by Gilman[4], is taken as the basis of the present development and has the form:

$$\dot{\epsilon}^P = \frac{1}{\tau}(\sigma/\sigma_0)^n \tag{2.1}$$

where τ, n and σ_0 are material constants (σ_0 is usually taken as the static yield stress), and σ is the actual stress.

By superposing the elastic part we have the complete constitutive relation:

$$\frac{\dot{\sigma}}{E} = \dot{\epsilon} - \frac{1}{\tau}\left|\frac{\sigma}{\sigma_0}\right|^n \operatorname{sign}(\sigma) \tag{2.2}$$

where $\operatorname{sign}(\sigma) = \begin{cases} 1 \text{ for } \sigma > 0 \\ -1 \text{ for } \sigma < 0 \end{cases}$, and E is Young's modulus. For constant strain rate loading, an asymptotic stress termed the dynamic yield stress σ_d exists and is given by

$$|\sigma_d/\sigma_0| = |\tau\dot{\epsilon}|^{1/n}. \tag{2.3}$$

Constitutive relations for elastic-viscoplastic materials under multiaxial deformation have been developed by Perzyna[5, 6] who again assumed that the total strain rate $\dot{\epsilon}_{ij}$ consists of an elastic part $\dot{\epsilon}^e_{ij}$ and an inelastic part $\dot{\epsilon}^P_{ij}$. Perzyna's theory assumes the existence of an initial yield surface beyond which viscoplastic flow occurs, the rate of increase of the viscoplastic strain components being a function of the extent to which the stress state exceeds the static yield criterion. Due to these assumptions, it is difficult to generalize one-dimensional viscoplastic models with no definite yield surface to multiaxial deformation using this theory. This difficulty is overcome by using a scalar flow potential $\Omega(\boldsymbol{\sigma}, \text{history})$ such that:

$$\dot{\epsilon}^P_{ij} = \frac{\partial\Omega(\boldsymbol{\sigma}, \text{history})}{\partial\sigma_{ij}} \tag{2.4}$$

where $\boldsymbol{\sigma}$ is the stress tensor. Examples of such constitutive models and their implications have been explored by Kelly and Gillis[3]. The following flow potential for nonhardening materials is used to generalize the one-dimensional theory:

$$\Omega = c\left(\frac{f(\boldsymbol{\sigma})}{f_0}\right)^{n+1} \tag{2.5}$$

where c is a material constant and $f(\boldsymbol{\sigma})$ equals f_0, a constant corresponding to the flow surface for static yielding. Thus

$$\dot{\epsilon}_{ij}^{P} = \beta^* \left(\frac{f(\boldsymbol{\sigma})}{f_0} \right)^n \frac{\partial f(\boldsymbol{\sigma})}{\partial \sigma_{ij}} \tag{2.6}$$

where $\beta^* = c(n+1)/f_0$. The complete constitutive relation is obtained by superposing the elastic part and inverting the resulting expression:

$$\dot{\boldsymbol{\sigma}} = \mathbf{D}^e \dot{\boldsymbol{\epsilon}} - \dot{\boldsymbol{\sigma}}^{(n)} \tag{2.7a}$$

where

$$\boldsymbol{\sigma} = \langle \sigma_{11} \sigma_{22} \sigma_{33} \sigma_{12} \sigma_{23} \sigma_{31} \rangle$$

$$\boldsymbol{\epsilon} = \langle \epsilon_{11} \epsilon_{22} \epsilon_{33} \epsilon_{12} \epsilon_{23} \epsilon_{31} \rangle$$

$\mathbf{D}^e$ – matrix of elasticity constants,

and

$$\dot{\boldsymbol{\sigma}}^{(n)} = \beta^* \mathbf{D}^e \left(\frac{f(\boldsymbol{\sigma})}{f_0} \right)^n \frac{\partial f(\boldsymbol{\sigma})}{\partial \boldsymbol{\sigma}}. \tag{2.7b}$$

For a von Mises type flow function,

$$f(\boldsymbol{\sigma}) = \sqrt{J_2(s)} = \left(\frac{1}{2} s_{ij} s_{ij} \right)^{1/2} \tag{2.7c}$$

and the nonlinear stress rate $\dot{\boldsymbol{\sigma}}^{(n)}$ simplifies to

$$\dot{\boldsymbol{\sigma}}^{(n)} = \beta \mathbf{D}^e \left(\frac{\sqrt{J_2}}{k} \right)^{n-1} \mathbf{s}/k \tag{2.7d}$$

where $\mathbf{s} = \langle s_{11} s_{22} s_{33} s_{12} s_{23} s_{31} \rangle^T$ is the deviatoric stress vector, k is the static yield stress in simple shear, and $\beta = \beta^*/2$. For uniaxial tension the constitutive relation (2.7) reduces to:

$$\dot{\sigma}/E = \dot{\epsilon} - (2\beta/\sqrt{3})(\sigma/\sigma_0)^n.$$

The constitutive model (2.7) describes all phases of deformation (elastic and elastic-viscoplastic, loading and unloading) in a smooth fashion and can be used to approximate elastic-perfectly plastic behavior in the limit as n approaches infinity† as suggested by Kelly[10]. Thus, there is no need to check loading or unloading processes nor to identify the state of the material during deformation when this constitutive model is incorporated in a numerical scheme, an advantage over models that assume a definite yield surface.

3. FINITE ELEMENT FORMULATION

The principle of virtual work[11, 12] and a finite element discretization are used to derive the following equations of motion[9]:

$$\mathbf{M}\, {}^k\ddot{\mathbf{q}}(t) + {}^k\mathbf{h} - {}^k\mathbf{R} = 0 \tag{3.1}$$

where $\mathbf{M}$ is the mass matrix, ${}^k\ddot{\mathbf{q}}(t)$ is the global nodal point acceleration vector, ${}^k\mathbf{R}$ is the external force vector, ${}^k\mathbf{h}$ is the equivalent nodal force vector, the superscript "k" denotes the current state, and t denotes the time parameter. The nodal forces are given by

$${}^k\mathbf{h}({}^k\mathbf{q}, {}^k\boldsymbol{\sigma}) = \int_{V_0} \mathbf{B}^T(\mathbf{x}, {}^k\mathbf{q})\, {}^k\boldsymbol{\sigma}\, \mathrm{d}V \tag{3.2}$$

where ${}^k\boldsymbol{\sigma}$ is as defined earlier, and $\mathbf{B}(\mathbf{x}, {}^k\mathbf{q})$ is the virtual global displacement- virtual strain

†In practice, a value of 25 or greater for n provides satisfactory results[9].

transformation matrix, i.e.

$$^{k}\delta\mathbf{E} = \mathbf{B}(\mathbf{x}, {}^{k}\mathbf{q})\,{}^{k}\delta\mathbf{q} \tag{3.3}$$

in which $^{k}\delta E = \langle {}^{k}\delta E_{11}\, {}^{k}\delta E_{22}\, {}^{k}\delta E_{33}\, 2{}^{k}\delta E_{12}\, 2{}^{k}\delta E_{23}\, 2{}^{k}\delta E_{31}\rangle^{T}$ is the vector of virtual Green strains, and the integral is carried over the original volume of the structure.

The equations of motion (3.1), the nodal force equations (3.2) together with appropriate constitutive relations and initial and boundary conditions constitute the system of equations governing the response of the finite element model. This type of formulation has been discussed by Argyris *et al.*[13] and Lukkunaprasit[9].

Incremental equations of motion

Of the numerous incremental methods available for solving nonlinear problems[14–16], a convenient approach is one in which the equations of motion (3.1) in a state "$k+1$" at time $t+\Delta t$ are expressed in terms of the adjacent state "k" at time t and the incremental quantities[9]:

$$\mathbf{M}\ddot{\mathbf{q}} + \mathbf{h}({}^{k}\mathbf{q}, \mathbf{q}, {}^{k}\boldsymbol{\sigma}) = {}^{k+1}\mathbf{R} - \mathbf{M}\,{}^{k}\ddot{\mathbf{q}} - {}^{k}\mathbf{h} \tag{3.4}$$

where

$$\mathbf{h}({}^{k}\mathbf{q}, \mathbf{q}, {}^{k}\boldsymbol{\sigma}) = \int_{V_0} \left[\mathbf{B}^{T}(\mathbf{x}, {}^{k}\mathbf{q})\boldsymbol{\sigma} + \frac{\partial B^{T}(\mathbf{x}, {}^{k}\mathbf{q})}{\partial {}^{k}\mathbf{q}}\, {}^{k}\boldsymbol{\sigma}\mathbf{q} \right] \mathrm{d}V \tag{3.5a}$$

$$\boldsymbol{\sigma} = {}^{k+1}\boldsymbol{\sigma} - {}^{k}\boldsymbol{\sigma}$$

$$\mathbf{q} = {}^{k+1}\mathbf{q} - {}^{k}\mathbf{q}.$$

Higher order terms are neglected in (3.5a). For elastic-viscoplastic materials with constitutive relations given by (2.7) the incremental nodal force $\mathbf{h}$ is:

$$\mathbf{h}({}^{k}\mathbf{q}, \mathbf{q}, {}^{k}\boldsymbol{\sigma}) = \mathbf{K}({}^{k}\mathbf{q}, {}^{k}\boldsymbol{\sigma})\mathbf{q} - \mathbf{h}^{(n)} \tag{3.5b}$$

where $\mathbf{K}$ is the incremental stiffness matrix given by

$$\mathbf{K}({}^{k}\mathbf{q}, {}^{k}\boldsymbol{\sigma}) = \int_{V_0} \left[\mathbf{B}^{T}\mathbf{D}^{e}\mathbf{B} + \frac{\partial \mathbf{B}^{T}}{\partial {}^{k}\mathbf{q}}\, {}^{k}\boldsymbol{\sigma} \right] \mathrm{d}V \tag{3.5c}$$

and

$$\mathbf{h}^{(n)} = \int_{V_0} \mathbf{B}^{T}\dot{\boldsymbol{\sigma}}^{(n)}\Delta t\, \mathrm{d}V. \tag{3.5d}$$

Due to the highly nonlinear nature of the material, the state $({}^{k+1}\mathbf{q}, {}^{k+1}\boldsymbol{\sigma})$ as obtained from one application of the incremental equations may not adequately satisfy the equations of motion (3.1). Therefore an iterative incremental procedure is adopted wherein the incremental equations of motion (3.4) are applied to the updated state, where k now denotes the updated state, $\mathbf{q}$ is the incremental displacement between two consecutive iterations, and $\mathbf{h}^{(n)}$ is modified to $\Delta\mathbf{h}^{(n)}$:

$$\Delta\mathbf{h}^{(n)} = \int_{V_0} \mathbf{B}^{T}\{\dot{\boldsymbol{\sigma}}^{(n)}(^{**}\boldsymbol{\sigma}) - \dot{\boldsymbol{\sigma}}^{(n)}(^{*}\boldsymbol{\sigma})\}\Delta t\, \mathrm{d}V \tag{3.6}$$

in which $^{*}\boldsymbol{\sigma}$ and $^{**}\boldsymbol{\sigma}$ are stress states within the time increment[9].

In our numerical scheme we neglect the term $\Delta\mathbf{h}^{(n)}$, which is acceptable provided that we iterate until convergence is achieved. Then, $^{k+1}\mathbf{R} - \mathbf{M}\,{}^{i}\ddot{q} - {}^{i}\mathbf{h}$ approaches zero as "i" approaches $k+1$, and the equations of motion (3.1) are satisfied.

Application to thin shells of revolution under axisymmetric loading

The theory described above will now be applied to thin plates and shells of revolution under torsionless axisymmetric loading. For simplicity we employ the conical frustum element[17] slightly modified to improve membrane characteristics. Figure 1 shows such an element

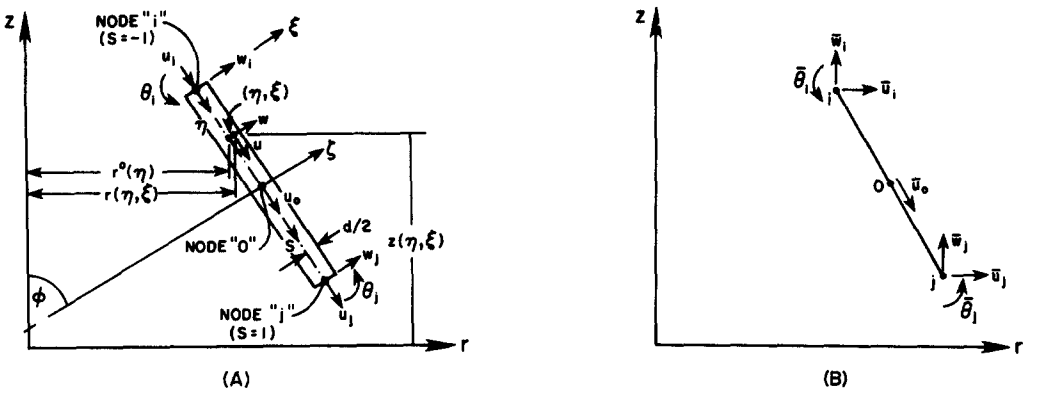

Fig. 1. Element geometry. (a) Conical frustum element—geometry and coordinate systems. (b) Midsurface nodal displacements in global coordinates.

together with the local physical coordinates (η, ξ), the local normalized coordinates (s, ζ), and the global coordinates (r, z). By adopting the Kirchhoff–Love hypothesis[18] the current meridional and normal displacement fields can be expressed in terms of those of the middle surface $u^0(\eta)$, $w^0(\eta)$ as follows:

$$\begin{aligned} u(\eta, \xi) &= u^0(\eta) - \xi w^0{}_{,\eta}(\eta) \\ w(\eta, \xi) &= w^0(\eta). \end{aligned} \tag{3.7}$$

The normal and in-plane displacement fields will be given by a cubic and quadratic representation, respectively:

$$\begin{aligned} u^0(s) &= s(s-1)/2u_i + (1+s)(1-s)u_0 + s(s+1)/2u_j \\ w^0(s) &= \psi_1(s)w_i + \psi_2(s)w_j + \psi_3(s)\theta_i + \psi_4(s)\theta_j \end{aligned} \tag{3.8}$$

where

$$\begin{aligned} \psi_1(s) &= 0.5 - 0.75s + 0.25s^3 \\ \psi_2(s) &= 0.5 + 0.75s - 0.25s^3 \\ \psi_3(s) &= L(1 - s - s^2 + s^3)/8 \\ \psi_4(s) &= L(-1 - s + s^2 + s^3)/8 \end{aligned}$$

L is the length of the element, $\underset{(j)}{u_i}$, $\underset{(j)}{w_i}$ and $\underset{(j)}{\theta_i}$ are respectively the meridional, normal displacement, and rotation of node "$\underset{(j)}{i}$", and u_0 is the meridional displacement of the center node "o". Due to axisymmetry of geometry and loading and the kinematic assumptions, the nonzero strain components are the meridional and circumferential strain components given, respectively, by:

$$\begin{aligned} k_{E_{\eta\eta}} &= u_{,\eta} + \frac{1}{2} w^2_{,\eta} \\ k_{E_{\theta\theta}} &= (u \cos \Phi + w \sin \Phi)/r \end{aligned} \tag{3.9}$$

where ϕ is the angle defining the element inclination (Fig. 1). We can easily deduce the strain-nodal displacement relations from local-global coordinate transformation[19]:

$$k_{E_{\eta\eta}}(s, \xi, {}^k\mathbf{q}) = \frac{2}{L}\langle\phi\rangle_{1,s}{}^k\mathbf{q} + \frac{1}{2}{}^k\mathbf{q}^T\langle\phi\rangle_3{}^T\langle\phi\rangle_3{}^k\mathbf{q} - \xi\left(\frac{2}{L}\right)^2\langle\phi\rangle_{2,ss}{}^k\mathbf{q}$$

$$k_{E_{\theta\theta}}(s, \xi, {}^k\mathbf{q}) = \frac{1}{r}[\langle\phi\rangle_1 \cos \Phi + \langle\phi\rangle_2 \sin \Phi - \xi\langle\phi\rangle_3 \cos \Phi]^k\mathbf{q}$$

$$\langle\phi\rangle_1 = \left\langle \frac{s(s-1)}{2}\cos\Phi, -\frac{s(s-1)}{2}\sin\Phi, 0, \frac{s(s+1)}{2}\cos\Phi, -\frac{s(s+1)}{2}\sin\Phi, 0, 1-s^2 \right\rangle$$

$$\langle\phi\rangle_2 = \langle\psi_1(s)\sin\Phi, \psi_1(s)\cos\Phi, \psi_3(s), \psi_2(s)\sin\Phi, \psi_2(s)\cos\Phi, \psi_4(s), 0\rangle$$

$$\langle\phi\rangle_3 = \frac{2}{L}\langle\phi\rangle_{2,s}$$

and

$${}^k\mathbf{q} = \langle\bar{u}_i, \bar{w}_i, \bar{\theta}_i, \bar{u}_j, \bar{w}_j, \bar{\theta}_j, u_0\rangle^T$$

is the vector of nodal displacements in global coordinates. Finally, by writing the above in terms of virtual quantities, we obtain:

$${}^k\delta\mathbf{E} = \mathbf{B}(s, \xi, {}^k\mathbf{q})^k\delta\mathbf{q}$$

$$\mathbf{B}(s, \xi, {}^k\mathbf{q}) = \begin{pmatrix} (2/L)\langle\phi\rangle_{1,s} + {}^k\mathbf{q}^T\langle\phi\rangle_3^T\langle\phi\rangle_3 \\ \dfrac{\langle\phi\rangle_1\cos\Phi + \langle\phi\rangle_2\sin\Phi}{r} \end{pmatrix} - \xi\begin{pmatrix} (4/L^2)\langle\phi\rangle_{2,ss} \\ \dfrac{\langle\phi\rangle_3\cos\Phi}{r} \end{pmatrix}$$

$$\equiv \mathbf{B}_{(1)}(s, {}^k\mathbf{q}) + \xi\mathbf{B}_{(2)}(s) \tag{3.10}$$

which is the matrix needed to evaluate the incremental stiffness matrix. The rates of strains and displacements are also related by the $\underline{B}$ matrix:

$${}^k\dot{\mathbf{E}} = \left[\mathbf{B}(s, \xi, {}^k\mathbf{q}) + \frac{\Delta t}{2}{}^k\dot{\mathbf{q}}^T\left(\frac{\partial\mathbf{B}^T(s, \xi, {}^k\mathbf{q})}{\partial^k\mathbf{q}}\right)^T\right]^k\dot{\mathbf{q}}. \tag{3.11}$$

4. FORMULATION IN TERMS OF STRESS RESULTANTS

We now introduce (3.10) into (3.2) to obtain the nodal force-internal stress resultant relations:

$${}^k\mathbf{h} = \sum^{\text{No of elements}}\left[\int_{-1}^{1}\left(B_{(1)}^T{}^k\mathbf{N}r^o(s)\frac{L}{2} + \mathbf{B}_{(2)}^T{}^k\mathbf{M}r^o(s)\frac{L}{2}\right)\mathrm{d}s\right] \tag{4.1}$$

in which

$${}^k\mathbf{N} = \int_{-d/2}^{d/2}\begin{Bmatrix} {}^k\sigma_{\eta\eta} \\ {}^k\sigma_{\theta\theta} \end{Bmatrix}\mathrm{d}\xi$$

$${}^k\mathbf{M} = \int_{-d/2}^{d/2}\begin{Bmatrix} {}^k\sigma_{\eta\eta} \\ {}^k\sigma_{\theta\theta} \end{Bmatrix}\xi\,\mathrm{d}\xi$$

d is the element thickness, and $r^o(s)$ has been used in place of $r(s, \xi)$ by the assumption of thin shells.

By virtue of the constitutive equations (2.7) and the rate of strain-displacement relations (3.11) the rates of the meridional and circumferential moment resultants, ${}^k\dot{M}_{\eta\eta}$ and ${}^k\dot{M}_{\theta\theta}$, at a section η are given by

$${}^k\dot{\mathbf{M}}(\eta) \equiv \begin{pmatrix} {}^k\dot{M}_{\eta\eta} \\ {}^k\dot{M}_{\theta\theta} \end{pmatrix} = \frac{d^3}{12}\mathbf{D}^e\mathbf{B}_{(2)}{}^k\dot{\mathbf{q}} - c_0\int_{-d/2}^{d/2}\left|\frac{\frac{1}{2}{}^k s_{ij}{}^k s_{ij}}{k^2}\right|^{(n-1)/2}\begin{pmatrix} 2\,{}^k\sigma_{\eta\eta} - {}^k\sigma_{\theta\theta} \\ -{}^k\sigma_{\eta\eta} + 2\,{}^k\sigma_{\theta\theta} \end{pmatrix}\xi\,\mathrm{d}\xi \tag{4.2}$$

where

$$c_0 = E\beta/[\sqrt{3}\sigma_0(1+\nu)],$$

and

$$\mathbf{D}^e = \frac{E}{1-\nu^2}\begin{pmatrix} 1 & \nu \\ \nu & 1 \end{pmatrix}. \tag{4.3}$$

The integrals in (4.2) involve nonlinear functions of the stresses which in turn are given by

nonlinear differential equations (2.7) and cannot be carried out explicitly. Our aim is to develop approximate expressions for these integrals. To do so, let us consider an elastic-perfectly plastic material. Theoretically, n tends to infinity for such a material. Prior to yielding, the function $1/2\,{}^k s_{ij}\,{}^k s_{ij}$ is less than the yield value k^2 at every point over the cross section, so that

$$\left|\frac{\frac{1}{2}\,{}^k s_{ij}\,{}^k s_{ij}}{k^2}\right|^{(n-1)/2}$$

and the integrals vanish in the limit as n tends to infinity.

Next, suppose that the section just reaches the limit (or plastic collapse) state, and thus that the yield condition $1/2\,{}^k s_{ij}\,{}^k s_{ij} = k^2$ is satisfied everywhere across the section. At this state, the yield condition in the stress resultant space can be derived [20] and symbolically represented by

$$f_y({}^k\mathbf{n}, {}^k\mathbf{m}) = 1 \tag{4.4}$$

where ${}^k\mathbf{n} = {}^k\mathbf{N}/N_0$; ${}^k\mathbf{m} = {}^k\mathbf{M}/M_0$; $N_0 = \sigma_0 d$; and $M_0 = \sigma_0 d^2/4$.

The local yield condition is replaced by the yield condition in the stress resultant space; thus,

$$\left|\frac{\frac{1}{2}\,{}^k s_{ij}\,{}^k s_{ij}}{k^2}\right|$$

may by replaced by

$$|f_y({}^k\mathbf{n}, {}^k\mathbf{m})|$$

so that (4.2) becomes

$$\begin{aligned} {}^k\dot{\mathbf{M}}(\eta) &= \frac{d^3}{12}\mathbf{D}^e\mathbf{B}_{(2)}{}^k\dot{\mathbf{q}} - c_0|f_y({}^k\mathbf{n}, {}^k\mathbf{m})|^{(n-1)/2}\int_{-d/2}^{d/2}\begin{pmatrix} 2\,{}^k\sigma_{\eta\eta} - {}^k\sigma_{\theta\theta} \\ -\,{}^k\sigma_{\eta\eta} + 2\,{}^k\sigma_{\theta\theta}\end{pmatrix}\xi\,\mathrm{d}\xi \\ &= \frac{d^3}{12}\mathbf{D}^e\mathbf{B}_{(2)}{}^k\dot{\mathbf{q}} - c_0|f_y({}^k\mathbf{n}, {}^k\mathbf{m})|^{(n-1)/2}\begin{pmatrix} 2\,{}^k M_{\eta\eta} - {}^k M_{\theta\theta} \\ -\,{}^k M_{\eta\eta} + 2\,{}^k M_{\theta\theta}\end{pmatrix} \end{aligned}$$

or in normalized form

$${}^k\dot{\mathbf{m}}(\eta) = \mathbf{D}_{(2)}\mathbf{B}_{(2)}{}^k\dot{\mathbf{q}} - c_0|f_y({}^k\mathbf{n}, {}^k\mathbf{m})|^{(n-1)/2}\,{}^k\mathbf{m}^* \tag{4.5a}$$

in which

$$\mathbf{D}_{(2)} = d^3\mathbf{D}^e/12M_0$$

and

$${}^k\mathbf{m}^* = \begin{pmatrix} 2\,{}^k m_{\eta\eta} - {}^k m_{\theta\theta} \\ -\,{}^k m_{\eta\eta} + 2\,{}^k m_{\theta\theta}\end{pmatrix}.$$

Equations (4.5a) are also valid at incipient yielding and will be adopted as interpolation functions, as shown schematically in Fig. 2 for one-dimensional bending of a beam section.

By the same procedure we arrive at the constitutive relations for the in-plane stress resultants:

$${}^k\dot{\mathbf{n}}(\eta) = \mathbf{D}_{(1)}\mathbf{B}_{(1)}{}^k\dot{\mathbf{q}} - c_0|f_y({}^k\mathbf{n}, {}^k\mathbf{m})|^{(n-1)/2}\,{}^k\mathbf{n}^* \tag{4.5b}$$

where

$$\mathbf{D}_{(1)} = d\mathbf{D}^e/N_0$$

and

$${}^k\mathbf{n}^* = \begin{pmatrix} 2\,{}^k n_{\eta\eta} - {}^k n_{\theta\theta} \\ -\,{}^k n_{\eta\eta} + 2\,{}^k n_{\theta\theta}\end{pmatrix}.$$

The foregoing treatment can be extended to the elastic-viscoplastic case by assuming that a viscoplastic collapse state exists for which the function $1/2\,{}^k s_{ij}\,{}^k s_{ij}$ takes on a value of k_d^2 throughout the cross section, where k_d is the dynamic yield value. The corresponding yield

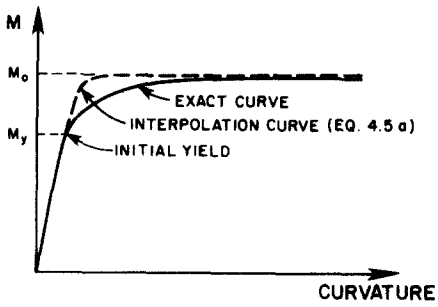

Fig. 2. Approximation of the actual elastic–plastic moment-curvature relation in beam bending.

surface in the stress resultant space is

$$f_y({}^k\mathbf{n}, {}^k\mathbf{m}) = \left(\frac{k_d}{k}\right)^2. \tag{4.6}$$

The function $1/2\,{}^k s_{ij}\,{}^k s_{ij}/k^2$ in eqns (4.2) is then replaced by $f_y({}^k\mathbf{n}, {}^k\mathbf{m})$ and the results are again eqns (4.5) but, of course, with different material constants than for the previous case. As before, eqns (4.5) are adopted as interpolation functions for intermediate states. It should be noted that in the stress resultant formulation only the *value* of the yield function $f_y({}^k\mathbf{n}, {}^k\mathbf{m})$ need be known. The flow condition has been incorporated in the constitutive relations for the stress components.

The yield condition in terms of stress resultants was first obtained by Ilyushin[21] in a parametric representation for the general thin shell obeying the von Mises yield criterion. Several cases where this relation could be expressed explicitly as a function of stress resultants were also given. By using the flow theory of plasticity, exact yield conditions for rotationally symmetric shells were derived by Onat and Prager[22] for Tresca materials and by Hodge[23] for von Mises yield criterion. Due to the complexity of these yield conditions, simplifying methods were introduced to obtain an approximate yield condition that was computationally manageable. Hodge[23, 24] replaced the uniform shell by an idealized sandwich shell. Approximations for the Tresca condition have been proposed by Flugge and Nakamura[25], Hodge[26] and others. Robinson[27] adopted the following yield conditions obtained by Ilyushin[21] for special cases as approximations to the whole yield surface, and obtained bounds for the collapse load associated with each case:

$$Y_1\colon J_2(\mathbf{n}) + J_2(\mathbf{m}) = 1; \qquad 0.955\,p_0 \le p_1 \le 1.155\,p_0$$

$$Y_2\colon J_2(\mathbf{m}) = [1 - J_2(\mathbf{n})]^2; \qquad 0.834\,p_0 \le p_2 \le p_0$$

$$Y_3\colon J_2(\mathbf{n}) + J_2(\mathbf{m}) + |J_{nm}|/\sqrt{3} = 1; \qquad 0.939\,p_0 \le p_3 \le 1.034\,p_0$$

where

$$J_2(n) = n_1^2 + n_2^2 - n_1 n_2 + 3n_{12}^2$$

$$J_2(m) = m_1^2 + m_2^2 - m_1 m_2 + 3m_{12}^2$$

$$J_{nm} = n_1\left(m_1 - \frac{m_2}{2}\right) + n_2\left(m_2 - \frac{m_1}{2}\right) + 3n_{12}m_{12}$$

n's and m's are, respectively, the nondimensional membrane and moment resultants, p_i is the collapse load corresponding to the yield condition Y_i, and p_0 is the exact collapse load. The approximate condition Y_1 was also obtained by Rozenblium[28] who used the lower and upper bound approach. Lukkunaprasit[9] arrived at Y_2 for the axisymmetric case by means of some physical and mechanical considerations and compared it to the exact von Mises condition given by Hodge[23]. The bounds for the collapse loads were:

$$0.854\,p_0 \le p_2 \le p_0.$$

Since the lower bound is slightly greater than that obtained by Robinson[27], Y_2 will be slightly more conservative for some deformation other than axisymmetric. More complicated higher order approximate yield conditions have been studied[27], but will not be discussed here.

5. NUMERICAL APPROACH TO NONLINEAR DYNAMIC PROBLEMS

Widely used direct integration operators in structural dynamics are the Houbolt[29], Newmark[30] and Wilson[31] operators. Their characteristics and unconditional stability criteria have been studied extensively with regard to their application to linear systems[30, 32–35]. Several A-stable methods for solving first order ordinary differential equations (o.d.e.) also exist[35, 36], but are less often used by structural engineers. An implicit second order Runge–Kutta method, with characteristics identical to the trapezoidal rule when applied to linear systems, will be employed in this study.

In applying integration operators to nonlinear systems, stability is governed not only by the integration operator used, but also by the method used to treat the nonlinear terms, and to some extent by the nature of the nonlinearity, e.g. geometric or material. In dealing with nonlinear vibrations of elastic shells, Stricklin *et al.*[37] treated the nonlinear terms as pseudo-generalized forces and used a linear extrapolation to obtain values at the end of the increment. Both the Newmark ($\gamma = 1/2$, $\beta = 1/4$) and Houbolt operators were investigated, and while the former was found to be unstable, the large artificial damping inherent in the latter method maintained stability. Wu and Witmer[38] employed a similar extrapolation procedure to solve for the dynamic response of an elastic–plastic beam under impulsive loading and reported less satisfactory results; even the Houbolt method ceased to maintain stability. Weeks[39] employed a Newton–Raphson iteration technique together with the Houbolt and Newmark methods for solving nonlinear problems and obtained very satisfactory results. However, all nonlinear terms were included explicitly in the equations of motion, requiring excessive storage for the Jacobian matrix generated by the Newton–Raphson procedure. Therefore, several difficulties, namely those of numerical stability, storage requirements, and practicality, must be resolved.

In the current state formulation it is convenient to decompose the equations of motion into a system of first order o.d.e.; thus:

$$\mathbf{M}\,{}^{k}\dot{\mathbf{v}} = {}^{k}\mathbf{R} - {}^{k}\mathbf{h} \tag{5.1}$$

$${}^{k}\mathbf{v} = {}^{k}\dot{\mathbf{q}}. \tag{5.2}$$

These equations, together with the constitutive relations (4.5), will be discretized using an implicit second order Runge–Kutta method[35], and the Newton–Raphson iteration scheme will be employed to solve the discretized algebraic equations.

To advance from the known state "k" to the next state "$k+1$", iterations $1, 2, \ldots, i, i+1, \ldots$ are performed, and the implicit Runge–Kutta scheme is applied to the equations of motion:

$$\mathbf{f}_v({}^{i}\mathbf{v}, {}^{i}\mathbf{h}) \equiv \mathbf{M}\frac{{}^{i}\mathbf{v} - {}^{k}\mathbf{v}}{\Delta t} - \frac{{}^{i}R + {}^{k}R}{2} + \frac{{}^{i}\mathbf{h} + {}^{k}\mathbf{h}}{2} = 0$$

where Δt is the time increment.

The residual is defined as:

$$\mathbf{f}_v({}^{i}\mathbf{v}, {}^{i}\mathbf{h}) \equiv \mathbf{M}\frac{{}^{i}\mathbf{v} - {}^{k}\mathbf{v}}{\Delta t} - \frac{{}^{i}\mathbf{R} + {}^{k}\mathbf{R}}{2} + \frac{{}^{i}\mathbf{h} + {}^{k}\mathbf{h}}{2} \tag{5.3}$$

which can be identified physically as the unbalanced nodal forces. With trial values ${}^{i}\mathbf{v}$, ${}^{i}\mathbf{h}$ the residual will in general be nonzero. The corrections $\Delta^{i}\mathbf{v} \equiv {}^{i+1}\mathbf{v} - {}^{i}\mathbf{v}$ and $\Delta^{i}\mathbf{h} \equiv {}^{i+1}\mathbf{h} - {}^{i}\mathbf{h}$ are sought to make $\mathbf{f}_v({}^{i+1}\mathbf{v}, {}^{i+1}\mathbf{h}) = 0$ by applying the Newton–Raphson scheme. Thus,

$$\mathbf{f}_v({}^{i}\mathbf{v} + \Delta^{i}\mathbf{v}, {}^{i}\mathbf{h} + \Delta^{i}\mathbf{h}) = 0 = \mathbf{f}_v({}^{i}\mathbf{v}, {}^{i}\mathbf{h}) + \frac{\partial \mathbf{f}_v}{\partial {}^{i}\mathbf{v}}\Delta^{i}\mathbf{v} + \frac{\partial \mathbf{f}_v}{\partial {}^{i}\mathbf{h}}\Delta^{i}\mathbf{h}$$

which, after introducing (5.3), yields:

$$\Delta^i\mathbf{v} = \Delta t\mathbf{M}^{-1}\left(-\mathbf{f}_v - \frac{\Delta^i\mathbf{h}}{2}\right). \tag{5.4}$$

As a first approximation $\Delta^i\mathbf{h}$ is taken as zero, equivalent to holding ${}^i\mathbf{h}$ fixed and allowing the velocity field to vary in such a way that the residual becomes zero.

By the procedures used before, the residual in the constitutive function is defined as:

$$\mathbf{f}_m({}^i\mathbf{m}, {}^i\mathbf{v}) = \frac{{}^i\mathbf{m} - {}^k\mathbf{m}}{\Delta t} - D_{(2)}B_{(2)}\frac{{}^i\mathbf{v} + {}^k\mathbf{v}}{2} + c_0 f_y^{(n-1)/2}(\bar{\mathbf{n}}, \bar{\mathbf{m}})\bar{\mathbf{m}}^* \tag{5.5}$$

in which the bar above a vector denotes the average values of the state "k" and the "i"th iterate. The Newton–Raphson method is applied to (5.5) with the velocity field fixed, resulting in [9]:

$$\begin{bmatrix} \frac{1}{\Delta t} + \frac{c_0}{2}a_1 & \frac{c_0}{2}a_1' \\ \frac{c_0}{2}a_2 & \frac{1}{\Delta t} + \frac{c_0}{2}a_2' \end{bmatrix} \begin{pmatrix} \Delta^i m_{\eta\eta} \\ \Delta^i m_{\theta\theta} \end{pmatrix} = -{}^i\mathbf{f}_m \tag{5.6}$$

where

$$c_1 = c_2' = 2; \quad c_1' = c_2 = -1.$$

$$\mathbf{a} = f_y^{(n-1)/2}\begin{pmatrix} c_1 \\ c_2 \end{pmatrix} + \begin{pmatrix} c_1\bar{m}_{\eta\eta} + c_1'\bar{m}_{\theta\theta} \\ c_2\bar{m}_{\eta\eta} + c_2'\bar{m}_{\theta\theta} \end{pmatrix}\frac{\partial f_y^{(n-1)/2}}{\partial \bar{m}_{\eta\eta}},$$

$$\mathbf{a}' = f_y^{(n-1)/2}\begin{pmatrix} c_1' \\ c_2' \end{pmatrix} + \begin{pmatrix} c_1\bar{m}_{\eta\eta} + c_1'\bar{m}_{\theta\theta} \\ c_2\bar{m}_{\eta\eta} + c_2'\bar{m}_{\theta\theta} \end{pmatrix}\frac{\partial f_y^{(n-1)/2}}{\partial m_{\theta\theta}}.$$

It can be shown that a_1 and a_2' are positive, and that $a_1a_2' > a_2a_1'$. It follows that the determinant of the coefficient matrix of $\Delta^i\mathbf{m}$ is nonzero and that an inverse exists. The in-plane stress resultants can be integrated in a similar manner.

Finally, the integration of (5.2) is simply

$${}^{i+1}\mathbf{q} - {}^k\mathbf{q} = \frac{{}^{i+1}\mathbf{v} + {}^k\mathbf{v}}{2}\Delta t.$$

No storage problems are created by applying the Newton–Raphson procedure to the global "linear" equations of motion (5.1) because (5.4) can be solved by Gaussian elimination or by other convenient alternative procedures. For nonlinear systems of equations (4.1) and (4.5) the finite element discretization technique allows the Newton–Raphson scheme to be applied locally at each section. Consequently, very little storage is required for the Jacobian matrix as is evident from (5.6).

A local stabilizing scheme for numerical solution of nonlinear equations

To stabilize the numerical integration of the system of nonlinear equations, a local step size subdivision stabilizing scheme is used in conjunction with the numerical integration method just described. Beginning with the incremental velocity predicted by (5.4), the residual in the constitutive functions and the change in internal stress at each Gauss station are calculated element-by-element. If the residual is large, the time step is subdivided into n equal subdivisions of duration $\Delta t_s = \Delta t/n$ for that Gauss station of the element (Fig. 3). If it is assumed that the variation of velocity within the time step is linear, then:

$${}^{j+1}\mathbf{v} = {}^j\mathbf{v} + \frac{{}^i\mathbf{v} - {}^k\mathbf{v}}{n}.$$

Given the velocity field, the numerical procedures discussed previously can be applied successively to each subdivision to determine the internal stresses at the end of each subdivision.

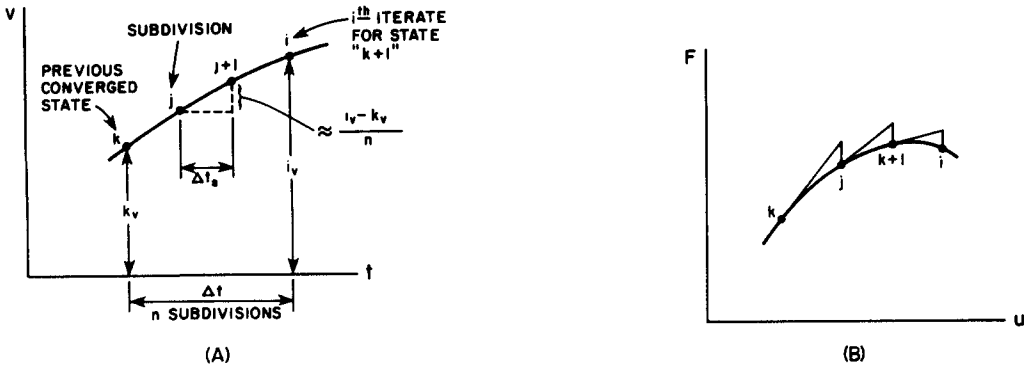

Fig. 3. Local time step subdivision scheme. (a) Velocity field. (b) Constitutive relation.

Where the material is elastic, the original procedure with large time steps is used. The internal stresses are then integrated numerically throughout the element to obtain the element nodal forces. By summing over all elements, the structural nodal forces are obtained and again introduced into the equations of motion, providing an improved solution $^{i+1}\mathbf{v}$. Iteration continues until convergence is achieved.

To illustrate the effectiveness of the local step size subdivision procedure, a single-story shear building subjected to base excitation as shown in Fig. 4 was considered. The columns are made of an elastic-perfectly plastic material and the column shear-displacement relation is approximated by an elastic-viscoplastic model:

$$\dot{F} = k\dot{u} - \frac{F_0}{\tau}\left(\frac{F}{F_0}\right)^n$$

where F is total story shear, F_0 is static yield value of total story shear, k is total elastic shear stiffness, u is story displacement and n and τ are material parameters. A large value, 51, was used for n and a value of 0.1 sec was assumed for τ.

A very small time step of approximately 1/74 T_1 where T_1 is the fundamental period for linear elastic vibration was used without applying the subdivision procedure and the scheme performed satisfactorily. Although some extremely small oscillations occurred in the story shear-displacement response during yielding (Fig. 5), the plot of story displacement vs time (Fig. 4) reveals that the steady state was accurately reproduced. This solution will be referred to as a converged solution.

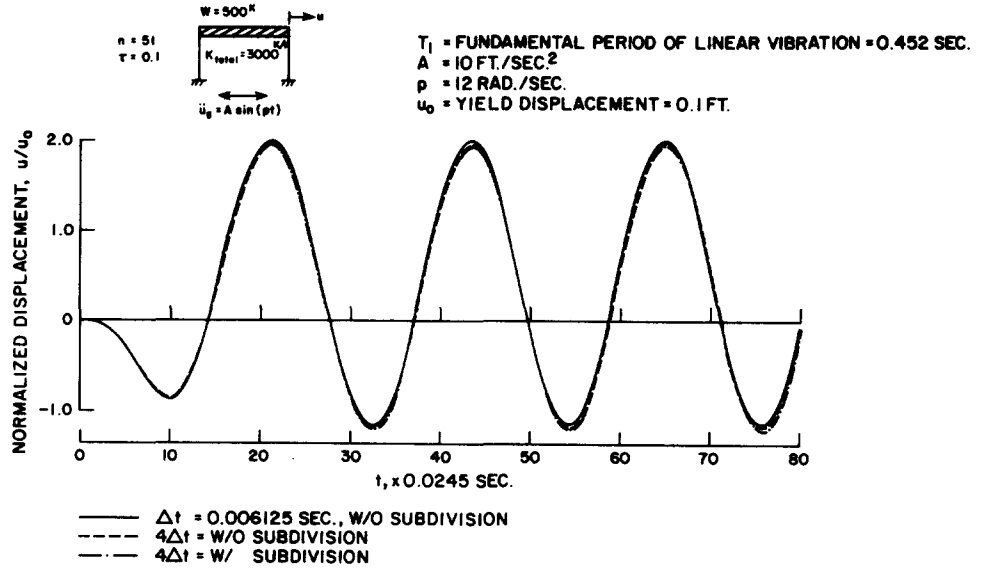

Fig. 4. Dynamic analysis of a shear building using a viscoplastic model—test of subdivision stabilizing scheme.

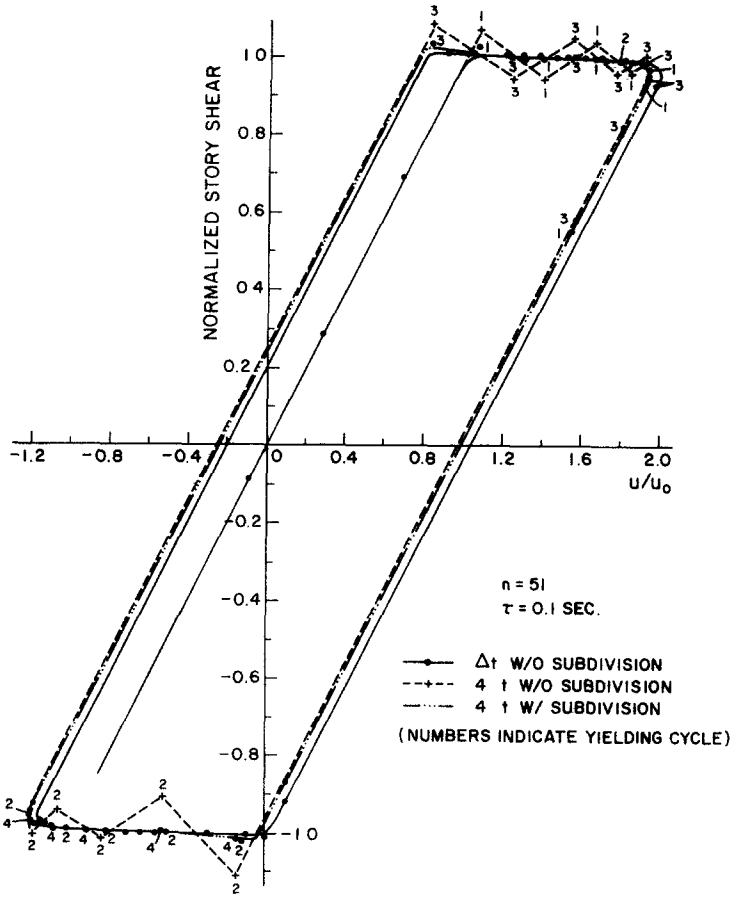

Fig. 5. Story shear—displacement diagram.

A time step four times the previous value was then used, still without using the subdivision procedure. The scheme functioned perfectly for the first 16 steps, during which the story shear was below the static yield level. During yielding, however, spurious oscillation occurred (see Fig. 5). Although the solution did not blow up, accuracy in the yielding regime was greatly reduced. Moreover, for problems such as impulsive loading of structures, it would be difficult to interpret the internal stress vs time response because real oscillations occur for such problems.

The difficulties described above were overcome by applying the subdivision procedure. With the large time step size as before and by subdividing the local time step into three once the constitutive residual exceeded 1.8, spurious oscillation was eliminated and the resulting solution compared very favorably with the converged solution (less than 4% maximum error). The error in peak displacement did not increase with time, indicating that the scheme did not introduce damping, either positive or negative. As in the linear case, a small error in phase occurred. It is evident from the story shear vs displacement diagram that a time step of 1/19 T_1 was rather large. Only three steps were required to stress the structure from a small negative shear force to a positive yield level, but the subdivision scheme maintained accuracy and stability.

6. NUMERICAL EXAMPLES

The incremental formulation developed herein was used to solve several dynamic problems in order to: (a) test the applicability and accuracy of the formulation, (b) develop an understanding of the behavior of the structural systems studied and (c) determine effects of mathematical modeling on structural response.

Impulsively loaded clamped circular plates

Several tests described in Ref. [40] were simulated using the present finite element model. In these experiments, the plates were clamped to prevent rotation but not radial displacement, and

Table 1. Material properties and plate geometry

Material	Static yield stress, psi. σ_0	Specific gravity	Plate radius	Plate thickness
AL 6061-T6	42,000	2.7	4.0 in.	0.251 in.
H.R. Steel A 285	41,080	7.8	4.0	0.245

were subjected to uniformly distributed impulses. The material properties and geometries of the aluminum and mild steel plates are given in Table 1.

Five elements were used to discretize half the plate. Geometric changes were accounted for in all analyses.

Idealization of materials

The aluminum alloy was assumed to be relatively rate insensitive. The material constants were: $n = 25$, $\tau = 0.00577$ sec, yielding, $\sigma_d = 1.06\,\sigma_0$ at $\dot{E} = 700\,\text{sec}^{-1}$.

The choice of constants for the steel was difficult since dynamic stress–strain rate tests were not carried out. Available experimental data with large variances had therefore to be used (see discussion by Perzyna[7]). Furthermore there is no standard value for strain-rate during a static test, so that the so-called "static yield stress" may differ among various laboratories. Therefore, two sets of material constants were chosen so that a wide range of dynamic stress–strain rate relationships could be represented (see Fig. 6): (1) $n = 17$, $\tau = 25{,}205$ sec, providing a good fit to Manjoine's curve[41], and (2) $n = 7$, $\tau = 0.75$ sec, approximating the experimental curve obtained by Clark and Duwez at low and medium strain rates[42].

Due to the difference in order of n and m in the yield function YF_2, the resulting constitutive model is more rate sensitive in bending when applied to rate-dependent materials. Therefore, the yield function $YF_1 = J_2(\mathbf{n}) + J_2(\mathbf{m})$ was used in all analyses but one.

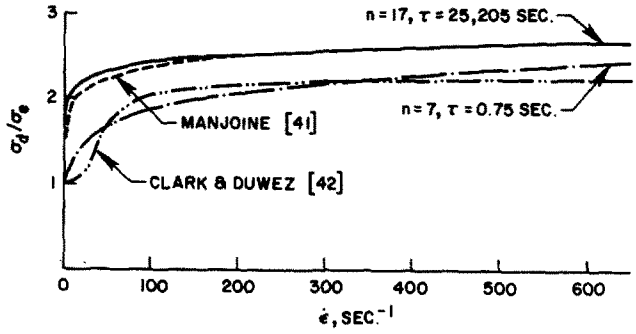

Fig. 6. Uniaxial dynamic yield stress–strain rate curves.

Idealization of impulsive loading

The applied impulse was idealized as a high pressure acting over a short duration t_p such that the product pt_p equaled the impulse. A very small pulse duration of 15 μs was used, based on the time required for the detonation at the center to reach the edge of the plate[40]. An equivalent pressure of more than 20 times the static collapse load (ps) was applied. According to Florence[43], an ideal impulse is closely approximated for large values of p/ps.

Some numerical aspects

The loading condition described above constitutes a rigorous test of the numerical schemes. Due to the high intensity and short duration of the pulse, yielding began almost instantaneously and higher mode response was significant. To capture the rapidly changing response with sufficient accuracy, a small time step of 3 μs was used. However, the time step should be increased once the fundamental mode becomes predominant. To prevent spurious oscillations in integrating the constitutive equations during time step changes, the subdivision procedure was employed. In one case, the time step was increased to 40 μs, about 1/13 the fundamental period of nonlinear vibration estimated from the free oscillation response, with satisfactory results.

Subdivisions were used whenever the value of the yield function exceeded 0.8. Two to four subdivisions sufficed.

Numerical results

(a) *Al. plates (relatively rate insensitive).* Two magnitudes of impulse were investigated, namely $I = 0.180$ and 0.228 psi-sec. The permanent deflection was estimated from the mean position of the free oscillation and compared to the experimental results [40] in Fig. 7 with very good agreement. The final plate profile for $I = 0.180$ psi-sec is shown in Fig. 8. The plate model was stiffer than the actual structure due to the approximation inherent in the stress resultant formulation and the coarse mesh discretization. The central deflection-time response for 100 integration steps is plotted in Fig. 9. During oscillation, the peak amplitude was reduced due to dissipation of plastic energy near stress reversals. Although the mechanism of deformation was extremely complex due to factors such as higher mode participation and interaction of membrane forces and bending moments, a general understanding of the mechanism can be gained by examining the variation of yield function values along the plate radius at different times (Fig. 10). Immediately after the impulse, plastic regions formed in the vicinity of $r/a = 0.81$ and 1 (support). These regions will be identified as negative and positive plastic regions according to the sign of the meridional moment. The rest of the plate remained elastic. Progressively, the plastic zone at the support spread and the negative plastic

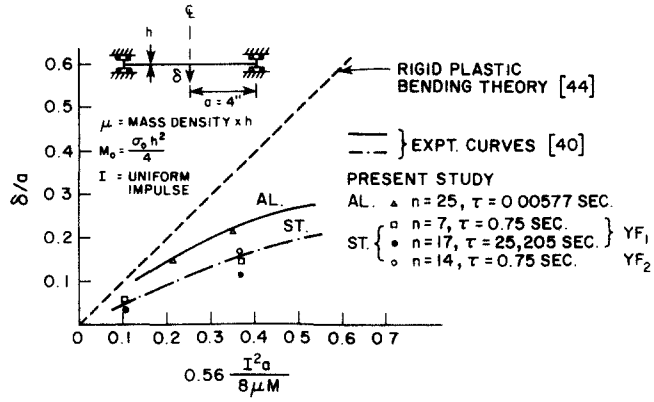

Fig. 7. Impulsive loading of clamped circular plates—comparison of finite element solutions to experimental results.

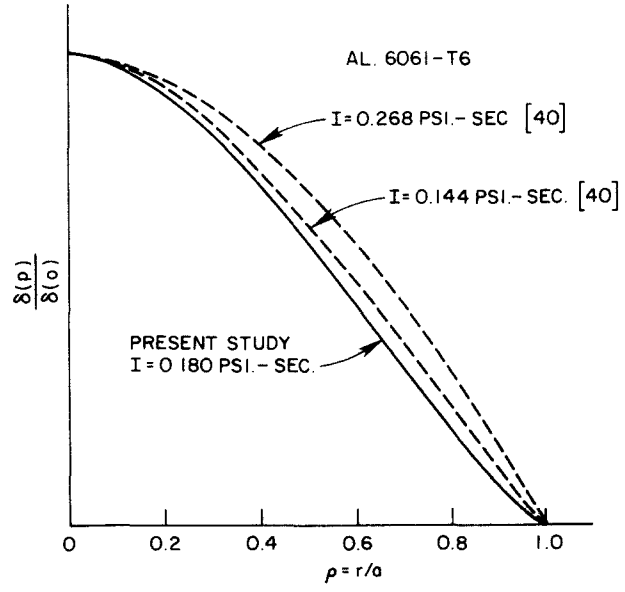

Fig. 8. Final plate profile.

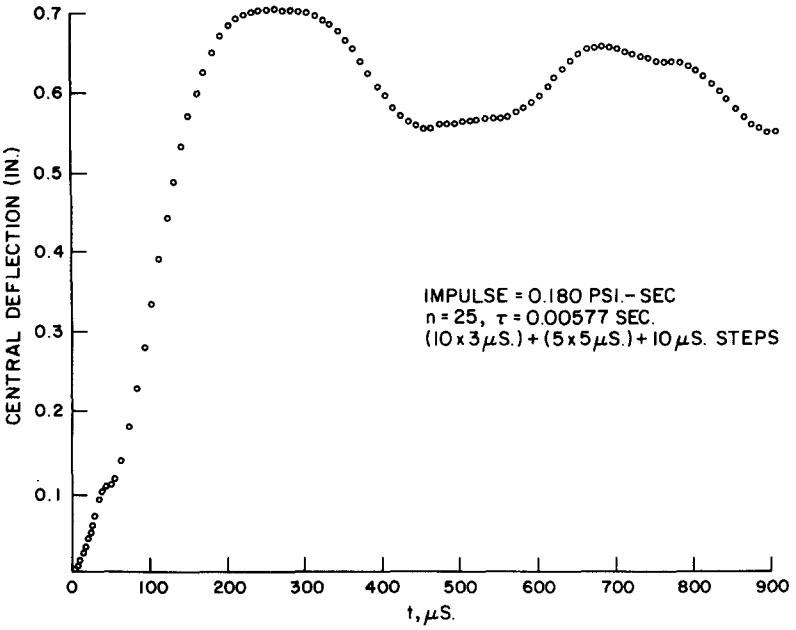

Fig. 9. Dynamic response of aluminum circular plate.

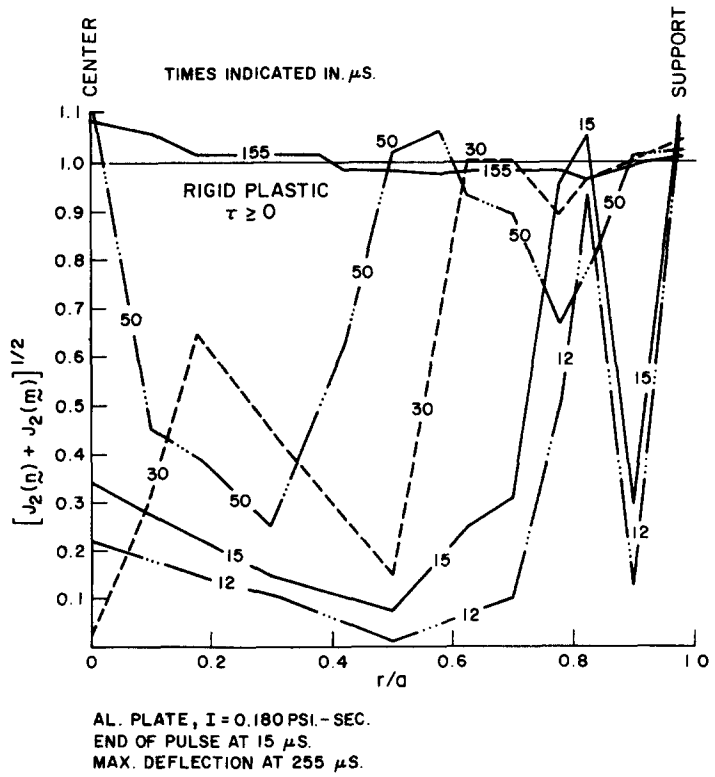

Fig. 10. Variation of values of the yield function along the radius at various times.

region moved toward the center, with an elastic region in between. The second phenomenon is analogous to the traveling plastic hinge of rigid-plastic analyses. It was not until $t = 155\,\mu s$ ($t_{\sigma_{max}} = 255\,\mu s$), when the entire plate had yielded, that general unloading occurred due to the contribution of membrane forces that had increased with increasing deflection. While the plate oscillated, a major portion remained elastic except for a small region near the support that was close to the yield level during reversals of the velocities. The plastic zones were highly localized for a considerable period of time while plastic deformation occurred. Loading and

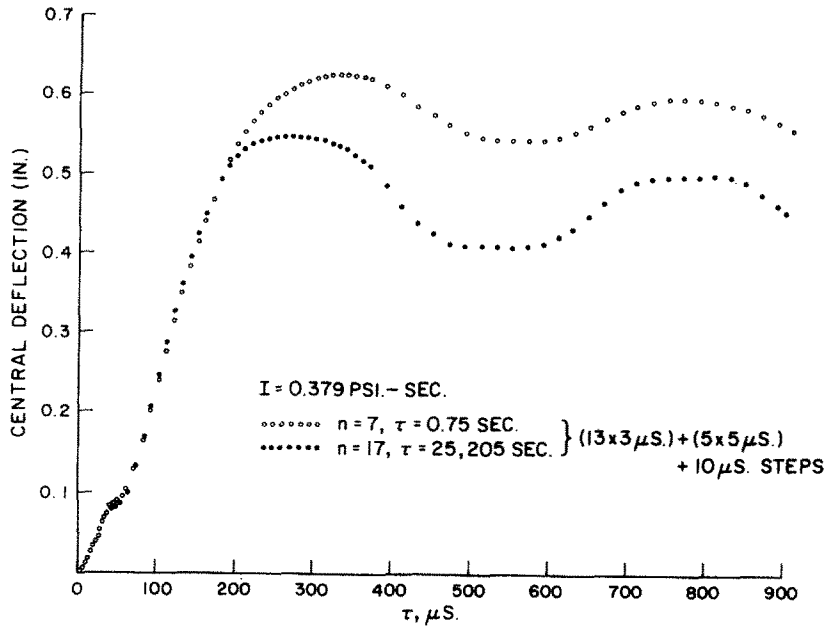

Fig. 11. Dynamic response of steel circular plates using different $\sigma_d - \epsilon$ curves.

unloading occurred in these zones due to the participation of higher modes that cannot be considered in rigid-plastic analyses.

(b) *Steel plates (rate sensitive).* The permanent central deflections for $I = 0.206$ and 0.379 psi-sec are shown in Fig. 7. The correlation with experimental data is not as good as for the perfectly plastic case because the response of viscoplastic materials depends on the idealization of $\sigma_d - \dot{E}$ behavior of the material over the entire range of strain rate during deformation. During the period of increasing deflection, strain rates were high (of the magnitude 300–1000 sec^{-1}) due to the high initial kinetic energy of the plate after the impulse was applied. Part of this energy was dissipated by plastic work so that free oscillation followed with lower strain rates (less than 100 sec^{-1}). If, for instance, the idealized dynamic yield stress is too high at some strain rate, then plastic flow will occur for higher stresses. Consequently, the material model will be too stiff and less deflection will result, as demonstrated in the plots of permanent central deflection as a function of time for the two material idealizations (Fig. 11). The lower $\sigma_d - \dot{E}$ curve ($n = 7$, $\tau = 0.75$ sec) resulted in a peak deflection 1.14 times that for the higher curve ($n = 17$, $\tau = 25{,}205$ sec). Furthermore, the amplitude of oscillation about the mean position was greater for the latter, indicating, as would be expected, less plastic dissipation.

Due to the problem associated with YF_2 as discussed earlier, the material parameters were selected from a pure-bending test. Thus, in order to fit the ($n = 7$, $\tau = 0.75$ sec) curve in Fig. 6, n and τ were taken as 14 and 0.75 sec, respectively, when YF_2 was used. The resulting permanent deflection (Fig. 7) was, as would be expected, greater by approximately 15% than the value predicted using YF_1.

Impulsively loaded shallow spherical shells

Shallow spherical shells with identical thickness, horizontally projected diameter, and boundary conditions as the circular plates treated previously were subjected to a uniform radial impulse with a magnitude of 0.379 psi-sec (Fig. 12). The material behavior was assumed to be characterized by the ($n = 7$, $\tau = 0.75$ sec) curve in Fig. 6. The idealization of impulses and time steps used in the plate problem were again assumed. Four shells with $\lambda = 1.5$, 3.0, 4.23 and 8.16 were investigated ($\lambda = a^2/Rh$ where $2a$ is equal to shell diameter, R is the radius of curvature and h is shell thickness), corresponding to half subtended angles (α) of 5.27, 10.6, 15.0 and 30°, respectively. Ten elements were used, except for the 10.6° shell which was the first to be analyzed using 8 elements. Changes in geometry were considered.

An integration time step as large as 20 μs, approximately 1/20 of the fundamental period of nonlinear vibration (T_1) for the 30° spherical shell, was used. To verify the accuracy of the solution, an analysis was performed with very small time steps on the order of 1/200 T_1 for the

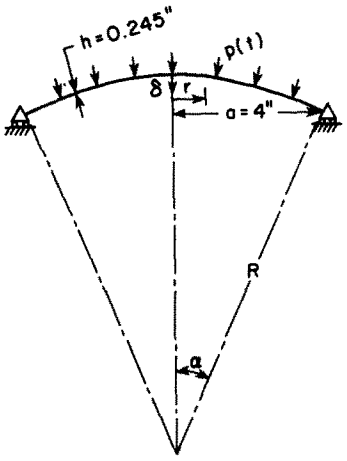

$E = 30 \times 10^6$ PSI., $\sigma_0 = 41{,}080$ PSI.
$\nu = 0.3$
$\rho = 0.000729$ LB. – $SEC.^2/IN.^4$

Fig. 12. Impulsive loading of shallow spherical shells.

30° shell. Resulting solutions are shown in Figs. 13 and 14. The central deflection increased slightly with smaller time steps. The maximum deflection differed by about 7%. Of the stress resultants, the meridional moment near the center fluctuated the most and was chosen for comparison. The agreement was generally good except during the early stage of response (about 3 times the pulse duration) at which very high-frequency modes prevailed. However, this result is not significant since the maximum moment associated with lower modes was predicted quite accurately using the larger time steps.

The predicted permanent central deflections are plotted in Fig. 15 with those for a circular plate. In contrast to what might have been expected, a very shallow shell ($\alpha <$ approximately 19°) underwent a deflection larger than that for a circular plate. This result can be explained as follows. A very shallow shell derives a major portion of load-carrying capacity from bending action. During the initial stage of response, however, such a shell is a softening structure due to the prevailing compressive membrane stress field. Only after membrane tensile stresses develop does the shell begin to stiffen due to membrane effect. On the other hand, a flat plate will

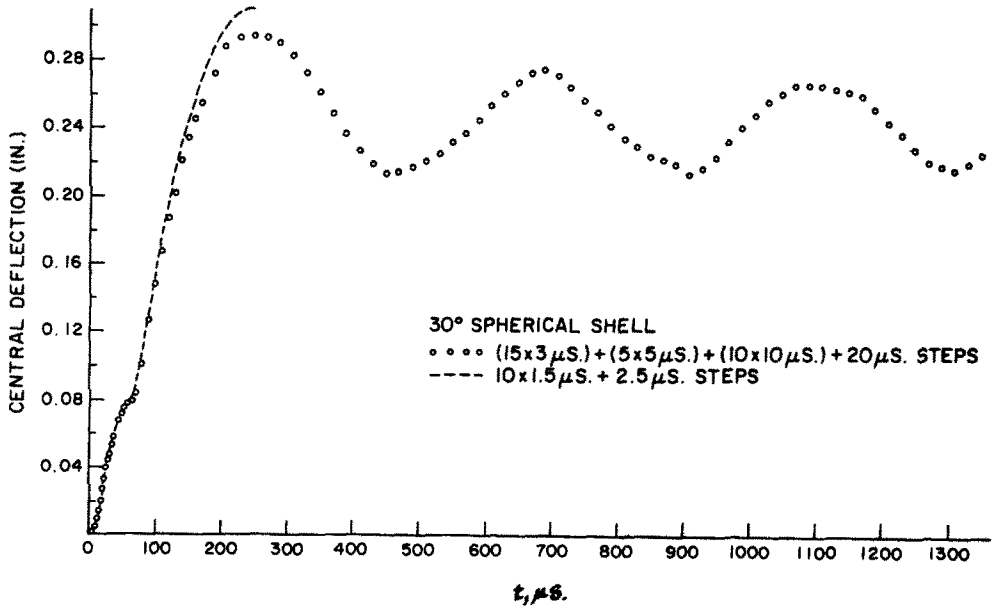

Fig. 13. Central deflection vs time for small and large time steps.

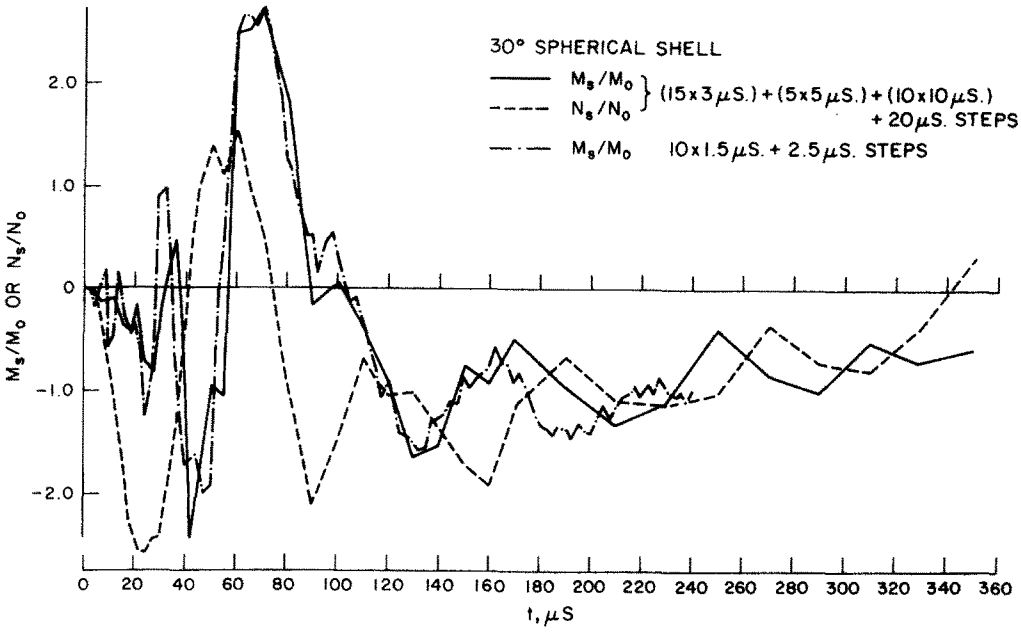

Fig. 14. Variation of moment and membrane force at $r/a = 0.00975$.

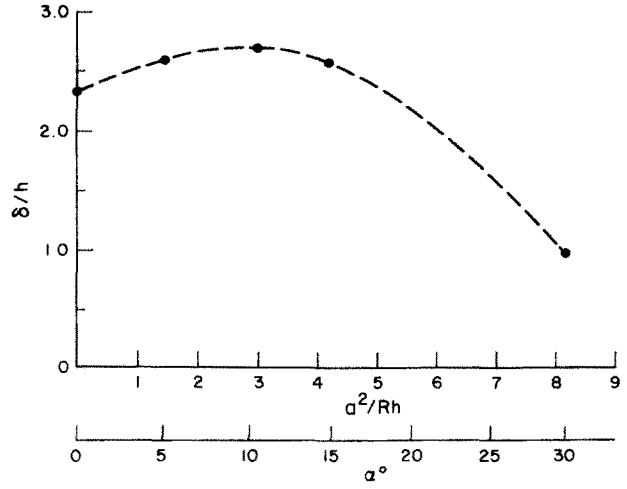

Fig. 15. Effect of shell geometry on permanent control deflection.

exhibit membrane strengthening behavior from the beginning. Therefore, a very shallow shell will deflect more under an identical loading. However, for deeper shells, shell action increasingly predominates and less deflection occurs.

7. CONCLUSIONS

The ability of the stress resultant finite element formulation to predict perfectly plastic collapse loads and elastic–plastic dynamic response of thin plates and shells of revolution has been demonstrated. Due to the inherent approximation introduced by the stress resultant formulation and the constitutive relation, the model is somewhat stiff in the elastic-partially plastic regime, but when plastic deformation predominates—the case when energy input is several times elastic strain energy of a structure—the stress resultant approach provides very satisfactory results.

The nonlinear elastic-viscoplastic model very effectively approximates elastic-perfectly plastic behavior when appropriate material parameters are chosen. In viscoplastic analysis, strain rate is extremely important. In structural dynamics, especially where impulsive loads or impacts are involved, strain rates can vary over a wide range, and predicted response will

depend on how well the constitutive model represents the actual (nonlinear) dynamic behavior of the material over the spectrum of strain rates involved. The nonlinear constitutive relation used in this study is simple, easy to use, and approximates dynamic yield stress–strain rate behavior reasonably well over a considerable range of strain rate.

An advantage of the approach used in the present stress resultant formulation is that only the value of the yield function need be known. Any yield condition may theoretically be used. However, in dynamic problems we find that the use of a homogeneous yield function eliminates apparent rate effects that are introduced when a nonhomogeneous yield function is used.

The example problems were a rigorous test of the numerical integration scheme, an implicit Runge–Kutta scheme with Newton–Raphson iteration, and the local time step subdivision procedure that were developed to improve the efficiency of the approach. These procedures were found to be very effective in handling the nonlinear constitutive relations. Predicted response was accurate even when very large time steps were used. No numerical damping was observed, but a small period error did occur. A computational advantage afforded by the local time step subdivision procedure is that it applies only to those elements currently yielding. The original time step is retained for all other elements during integration of the equations of motion. During a change in time step size, the procedure was effective in suppressing oscillations. This local time step subdivision concept should be valuable in the conventional plasticity formulations as well since it allows the history-dependent response of materials to be traced with greater accuracy.

Although not studied in detail, a rough comparison of computational time required to solve a typical problem revealed that for the same degree of accuracy, the present formulation required approximately one-half as much time as a conventional stress component finite element formulation using perfectly plastic theory. Furthermore, the formulation is readily applicable to analyses of nonlinear creep problems since the form of the constitutive relations would remain the same. Shearing effects can be included in both the kinematic of deformation and yield conditions, so that moderately thick shells could be analyzed. The constitutive relations could be modified to include strain-hardening and thermal effects. To extend the method to large displacement analysis would require only slight modifications to incorporate appropriate constitutive relations for finite deformation and to account for the effects of geometric changes in calculating nodal forces. The simplicity, versatility, and accuracy of the formulation make it attractive for use in design offices as well as in research.

Acknowledgement—The research reported herein was partially supported by National Science Foundation Grant ENV76–04262.

REFERENCES

1. V. V. Sokolovsky, Propagation of elastic-viscoplastic waves in bars. *Prikl. Mat. Mekh.* **12**, 261–280 (1948) (In Russian).
2. L. E. Malvern, The propagation of longitudinal waves of plastic deformation in a bar of material exhibiting a strain-rate effect. *J. Appl. Mech.* **18**, 203–208 (1951).
3. J. M. Kelly and P. P. Gillis, The influence of a limiting dislocation flux on the mechanical response of polycrystalline metals. *Int. J. Solids Structures* **10**, 45–59 (1974).
4. J. J. Gilman, *Micromechanics of Flow in Solids*. McGraw-Hill, New York (1969).
5. P. Perzyna, The constitutive equations for rate sensitive plastic materials. *Q. Appl. Math.* **20**, 321–322 (1963).
6. P. Perzyna, The constitutive equations for work-hardening and rate sensitive materials. *Proc. Vibr. Prob.* **4**, 281–290 (1963).
7. P. Perzyna, Fundamental problems in viscoplasticity. *Advances in Applied Mechanics*, Vol. 9, pp. 244–377. Academic Press, New York (1966).
8. E. O. Hall, *Yield Point Phenomena in Metals and Alloys*. Macmillan, New York (1970).
9. P. Lukkunaprasit, Dynamic Analysis of Elastic-Viscoplastic Plates and Shells of Revolution Using a Stress Resultant Finite Element Formulation. Ph.D. Dissertation, Department of Civil Engineering, University of California, Berkeley (1974).
10. J. M. Kelly, An elastic plastic shell theory for the analysis of millimeter wave guide strengthening process. *Bell Telephone Lab. Rep.* (1973).
11. S. Yaghami, Incremental Analysis of Large Deformations in Mechanics of Solids with Application to Axisymmetric Shells of Revolution. Ph.D. Dissertation, Department of Civil Engineering, University of California, Berkeley (1968).
12. K. Washizu, *Variational Methods in Elasticity and Plasticity*. Pergamon Press, New York (1968).
13. J. H. Argyris, P. C. Dunne and T. Angelopoulos, Non-linear oscillations using the finite element technique. *Comp. Meth. Appl. Mech. Engng* **2**, 203–250 (1973).
14. C. A. Felippa, Refined Finite Element Analysis of Linear and Nonlinear Two-Dimensional Structures. Ph.D. Dissertation, Department of Civil Engineering, University of California, Berkeley (1966).
15. H. D. Hibbit, P. V. Marcal and J. R. Rice, A finite element formulation for problems of large strain and large displacements. *Int. J. Solids Structures* **6**, 1069–1086 (1970).

16. J. T. Oden, *Finite Elements of Nonlinear Continua*. McGraw-Hill, New York (1972).
17. Z. A. Lu, J. Penzien and E. P. Popov, Finite element solution for thin shells of revolution. *J. Engng Mech. Div. ASCE* **90**(EM5), 119–145 (1964).
18. S. Timoshenko and S. Woinowsky-Krieger, *Theory of Plates and Shells*. McGraw-Hill, New York (1959).
19. O. C. Zienkiewicz, *The Finite Element Method in Engineering Science*. McGraw-Hill, New York (1971).
20. P. G. Hodge, *Limit Analysis of Rotationally Symmetric Plates and Shells*. Prentice-Hall, Englewood Cliffs, New Jersey (1963).
21. A. A. Ilyushin, *Plasticity*. Gostekhizdat, Moscow (1948) (in Russian); *Plasticité*. Eyrolles, Paris (1956) (in French).
22. E. T. Onat and W. Prager, Limit analysis of shells of revolution. *Proc. Netherlands Acad. Sci.* **B57**, 534–548 (1954).
23. P. G. Hodge, The Mises yield condition for rotationally symmetric shells. *Q. Appl. Math.* **18**, 305–311 (1961).
24. P. G. Hodge, The rigid-plastic analysis of symmetrically loaded cylindrical shells. *J. Appl. Mech.* **21**, 336–342 (1954).
25. W. Flugge and T. Nakamura, Plastic analysis of shells of revolution under axisymmetric loads. *Ingenieur-Archiv.* **34**, 238–247 (1965).
26. P. G. Hodge, Yield conditions for rotationally symmetric shells under axisymmetric loading. *J. Appl. Mech.* **27**, 323–331 (1960).
27. M. Robinson, A comparison of yield surfaces for thin shells. *Int. J. Mech. Sci.* **13**, 345–354 (1971).
28. V. I. Rozenblium, Plasticity conditions for thin shells. *Prikl. Mat. Mekh.* **24**, 264–372 (1960).
29. J. C. Houbolt, A recurrence matrix solution for the dynamic response of elastic aircraft. *J. Aero. Sci.* **17**, 540–550 (1950).
30. N. M. Newmark, A method of computation for structural dynamics. *J. Engng Mech. Div. ASCE* **85**(EM3), 67–94 (1959).
31. E. L. Wilson, A Computer Program for the Dynamic Stress Analysis of Underground Structures. *SESM Rep. No.* 68–1, Department of Civil Engineering, University of California, Berkeley (1968).
32. G. L. Goudreau and R. L. Taylor, Evaluation of numerical integration methods in elasto-dynamics. *Comp. Meth. Mech. Engng* **2**, 69–97 (1973).
33. R. E. Nickell, On the stability of approximation operators in problems of structural dynamics. *Int. J. Solids Structures* **7**, 301–319 (1972).
34. R. E. Nickell, Direct integration methods in structural dynamics. *J. Engng Mech. Div. ASCE* **93**(EM2), 303–317 (1973).
35. L. Lapidus and J. H. Seinfield, *Numerical Solution of Ordinary Differential Equations*. Academic Press, New York (1971).
36. G. G. Dahlquist, A special stability problem for linear multi-step methods. *Nordisk Tidskrift Informationsbehandling* **3**, 27–43 (1963).
37. J. A. Stricklin *et al.*, Nonlinear dynamic analysis of shells of revolution by the matrix displacement method. *AIAA J.* **9**, 629–636 (1971).
38. R. W.-H. Wu and E. A. Witmer, Nonlinear transient response of structures by the spatial finite element method. *AIAA J.* **11**, 1110–1117 (1973).
39. G. E. Weeks, Temporal operators for nonlinear structural dynamics problems. *J. Engng Mech. Div. ASCE* **98**(EM5), 1087–1104 (1972).
40. Y. Wierzbicki and A. L. Florence, A theoretical and experimental investigation of impulsively loaded clamped circular viscoplastic plates. *Int. J. Solids Structures* **6**, 553–568 (1970).
41. M. Manjoine, Influence of rate of strain and temperature on yield stresses of mild steel. *J. Appl. Mech.* **11**, 211–218 (1944).
42. D. S. Clark and P. E. Duwez, The influence of strain rate on some tensile properties of steel. *Proc. ASTM* **50**, 560–575 (1950).
43. A. L. Florence, Clamped circular rigid-plastic plates under central blast loading. *Int. J. Solids Structures* **2**, 319–335 (1966).
44. A. J. Wang and H. G. Hopkins, On the plastic deformation of built-in circular plates under impulsive load. *J. Mech. Phys.* **3**, 22–37 (1954).